

Landau-Ginzburg Perspective of Finite-Temperature Phase Diagrams of a Two-Component Fermi-Bose Mixture

Michael Fodor and Hong Y. Ling

Department of Physics and Astronomy, Rowan University, New Jersey 08028-1700

Abstract

We consider a mixture of two-component Fermi and (one-component) Bose gases under the repulsive Bose-Fermi and attractive Fermi-Fermi interaction. We perform a systematic study of the finite-temperature phase diagrams in the chemical potential space, identifying, using the Landau-Ginzburg theory, the features generic to the phase diagrams within the validity of our model. We apply the theory to explore the physics of correlated BCS pairing among fermions in a tightly confined trap surrounded by a large BEC gas.

PACS: 67.85.-d, 03.75.Ss, 03.75.Mn

I. INTRODUCTION

Fermions, constrained by the Pauli exclusion principle, behave very differently from bosons, to which such a principle does not apply. In a many particle system, the former tend to stay away from each other, while, on the contrary, the latter tend to be gregarious. In the most fundamental level, fermions (leptons and quarks) are the building block for all the matter with mass, while bosons serve as the mediator for all the fundamental forces in nature. In spite of this vast difference, when mixed together at temperatures so low that the de Broglie wavelength of the particles becomes comparable to or even longer than the interparticle spacing, fermions and bosons can conspire to create fascinating quantum effects at the macroscopic scale that are of fundamental interest across a broad spectrum of physics, especially within the disciplines of condensed matter and nuclear physics. As most substances in nature solidify before the temperature could reach the regime where the macroscopic quantum nature of liquid (or gas) can be manifested, the combination of liquid isotopes between ^3He and ^4He [1] has remained the only laboratory accessible system until recently when the rapid technological advancement in cooling and trapping of neutral atoms has completely turned the situation around. Not only has it resulted in a dramatic proliferation of such systems, including ^6Li - ^7Li [2, 3], ^6Li - ^{23}Na [4], ^{87}Rb - ^{40}K [5–8], ^6Li - ^{87}Rb [9], but more significantly, with ultracold atomic gases, important parameters, including the interaction between particles of same or different species, can be tuned precisely [7–10], allowing the physics of Fermi-Bose mixture to be investigated in a well controlled manner, in regimes possibly well beyond the reach by traditional solid state systems.

Recently, by changing the Feshbach detuning across a certain critical point at which all the minority atoms pair up with the majority ones to form a molecular Bose condensate, the group at MIT [11] has successfully created, from a two-component Fermi mixture with population imbalance, a quantum gas where Bose molecules are mixed with spin-polarized (unpaired majority) fermions. In addition to confirming an earlier theoretical prediction of the existence of a transition from full miscibil-

ity to phase separation [12, 13], using the same system, they were able to determine the effective dimer-fermion scattering length within a reasonable agreement with the prediction made more than 50 years ago [14] but never verified experimentally, once again demonstrating that the ultracold atom system provides an excellent experimental platform for testing theories.

Inspired by this work, instead of one Fermi state as in a single-component Fermi-Bose mixture in Ref. [11], we consider a two-component Fermi-Bose mixture involving a hyperfine state $|b\rangle$ of a bosonic atom with mass m_B and two equally populated hyperfine states: spin up $|\uparrow\rangle$ and spin down $|\downarrow\rangle$ of a fermionic atom with mass m_F . The latter Fermi system when equipped with Feshbach resonance has been the main source of inspiration for much recent excitement in the forefront of ultracold atomic physics, due chiefly to the vital role it plays in the study of crossover from Bose-Einstein condensation (BEC) of tightly bound atom pairs to nonlocal Bardeen-Cooper-Schrieffer (BCS) atom pairs. Thus, mixtures of bosons with such Fermi systems shall be widely accessible to experiments.

The low temperature physics of the two-component model under consideration is dominated by s -wave collisions, which, given that the Pauli exclusion principle prohibits s -wave scattering between identical fermions, are parameterized with three scattering lengths: a_{BB} , a_{FF} , and a_{BF} , describing, respectively, s -wave scattering between two bosons, between two fermions of opposite spins, and between a boson and a fermion of either spin, assuming that scattering a boson off a spin-up fermion has the same amplitude as that off a spin-down fermion. In principle, a_{BB} must be positive necessitated by the Bose stability in the mixture, while a_{BF} and a_{FF} can take both positive and negative values as they are not subject to similar constraints. Thus, in spite of the restriction on a_{BB} , such a model can still represent drastically different regimes of physics as far as pairings and instabilities are concerned. In the present work, we aim to extend the physics of phase and phase separation at finite temperature from single- to two-component systems where fermions have the opportunity to form correlated BCS pairs. As a result, we limit our study to systems with repulsive ($a_{BF} > 0$) Bose-Fermi and at-

tractive ($a_{FF} < 0$) Fermi-Fermi interaction.

In Sec. II, we review, within the framework of mean-field theory, the path integration formulation of the finite-temperature thermodynamic potential and derive from it the Landau-Ginzburg expansion. In contrast to the existing works for the two-component model [15–17], which have various purposes, we focus on producing phase diagrams in the space made up of chemical potentials, which are intensive statistical variables that must remain invariant among the separated phases and hence uniquely define a phase separation [19]. This is to be contrasted to spaces where coordinates are served, for example, by particle number densities, of which separated phases in a phase separation have different values [15, 18]. In Sec. III, we apply the analytical intuitions derived from the Landau-Ginzburg theory to identify as well as to clarify the features that are generic to the finite-temperature phase diagrams within the validity of our model. The utility of such phase diagrams can be most easily appreciated when one wants to map out the particle number densities for a trapped model where the local density approximation holds. An example will be shown in Sec. IV, which illustrates how the surrounding large BEC affects the physics of pairing among fermions in a tightly confined trap. Finally, we provide a short conclusion and discussion in Sec. V.

II. MEAN-FIELD THERMODYNAMIC POTENTIAL AND LANDAU-GINZBURG EXPANSION

The thermodynamic properties of our model can be described by the partition function Z , which is a functional integral over both the complex fields for bosons: $\psi_{\mathbf{k},B}(\tau)$ and $\psi_{\mathbf{k},B}^*(\tau)$ and the Grassman fields for fermions: $\psi_{\mathbf{k},\sigma}(\tau)$ and $\bar{\psi}_{\mathbf{k},\sigma}(\tau)$ in the momentum ($\hbar\mathbf{k}$) and imaginary time (τ) space [20]. In this work, we limit our study to the regime of temperature far below $T_B = 2\pi\hbar^2 [n_B/\zeta(3/2)]^{2/3} / (m_B k_B)$, where n_B is the Bose atom number density, k_B the Boltzman constant, and $\zeta(x)$ the Riemann-Zeta function. In this limit, bosons are virtually all condensed to the zero momentum mode, and the standard symmetry breaking ansatz, $\psi_{\mathbf{k},B}(\tau) = \psi_{\mathbf{0},B} + \phi_{\mathbf{k}\neq\mathbf{0},B}(\tau)$, is therefore applicable, where $\psi_{\mathbf{0},B}$ is a classical field (not part of the path integration variable) for condensed particles, and $\phi_{\mathbf{k},B}(\tau)$ is a bosonic field for condensate excitations or simply phonons for a dilute gas where the usual Bogoliubov approximation holds [16]. Further, for pedagogical reason, we opt to first ignore all the phonon degrees of freedom, justifying, however, in the end of the paper, that the ensuing formalism, when appropriately modified, can be applied for a large class of Fermi-Bose mixtures where the effects of phonons are included.

The grand partition function Z , at temperature T ($\equiv 1/k_B\beta$), boson chemical potential μ_B , and fermion chemical potential μ_F , then reads $Z = \int D[\bar{\psi}, \psi] \exp(-S[n_B, \bar{\psi}, \psi]/\hbar)$, where $n_B = |\psi_{\mathbf{0},B}|^2/V$

is the boson number density, V the total volume, S the action given by

$$S = \hbar\beta V \left(\frac{g_{BB}}{2} n_B^2 - \mu_B n_B \right) + \int_0^{\hbar\beta} d\tau \left[\sum_{\mathbf{k},\sigma} \bar{\psi}_{\mathbf{k},\sigma} \left(\hbar \frac{\partial}{\partial \tau} + \xi_{\mathbf{k}} \right) \psi_{\mathbf{k},\sigma} + \frac{U}{V} \sum_{\mathbf{k},\mathbf{k}',\mathbf{q}} \bar{\psi}_{\mathbf{k},\uparrow} \bar{\psi}_{\mathbf{q}-\mathbf{k},\downarrow} \psi_{\mathbf{k}',\downarrow} \psi_{\mathbf{q}-\mathbf{k}',\uparrow} \right] \quad (1)$$

In arriving at Eq. (1), we have incorporated the interaction between fermions and bosons into Eq. (1) via $\xi_{\mathbf{k}} = \epsilon_{\mathbf{k}} - \mu$ in terms of the effective fermion chemical potential $\mu = \mu_F - g_{BF} n_B$, where $\epsilon_{\mathbf{k}} = (\hbar k)^2 / 2m_F$ is the kinetic energy of a fermion with a momentum $\hbar\mathbf{k}$, and $g_{BB} = 4\pi\hbar^2 a_{BB}/m_B$ and $g_{BF} = 4\pi\hbar^2 a_{BF}/m_{BF}$ measure the strengths of respective s-wave scatterings with $m_{BF} = 2m_B m_F / (m_B + m_F)$, and we have also modeled the interaction between fermions of opposite spins with the parameter U , which, in the actual calculation, will be replaced in favor of the physical parameter U_0 ($= 4\pi\hbar^2 a_{FF}/m_F$) via the standard renormalization relation $U^{-1} = U_0^{-1} - \sum_{\mathbf{k}} \epsilon_{\mathbf{k}}^{-1} / (2V)$.

In anticipation of the BCS pairing as a result of an attractive fermion-fermion interaction, we follow the standard procedure in which we first introduce the auxiliary bosonic fields Δ and Δ^* (assuming they are uniform and static) and then apply the Hubbard-Stratonovic decomposition to change the partition function into $Z = \int D[\bar{\psi}, \psi, \Delta^*, \Delta] \exp(-S'[n_B, \bar{\psi}, \psi, \Delta^*, \Delta]/\hbar)$, where the action

$$S' = \hbar\beta \left[V \left(\frac{g_{BB}}{2} n_B^2 - \mu_B n_B \right) - V \frac{|\Delta|^2}{U} + \sum_{\mathbf{k}} \xi_{\mathbf{k}} \right] + \sum_{\mathbf{k}, i\omega_n} \bar{\psi}_{\mathbf{k}, i\omega_n} \begin{pmatrix} -i\hbar\omega_n + \xi_{\mathbf{k}}, & \Delta \\ \Delta^*, & -i\hbar\omega_n - \xi_{\mathbf{k}} \end{pmatrix} \psi_{\mathbf{k}, i\omega_n}, \quad (2)$$

is expressed in terms of Nambu spinor $\psi_{\mathbf{k}, i\omega_n} = (\psi_{\mathbf{k}, i\omega_n, \uparrow}, \bar{\psi}_{-\mathbf{k}, -i\omega_n, \downarrow})^T$, with $\psi_{\mathbf{k}, i\omega_n, \uparrow}$ or \downarrow being the field components in the imaginary (Matsubara) frequency $i\omega_n$ space.

Finally, by integrating out fermionic fields and carrying out a summation over the Matsubara frequency, we arrive, within the saddle point approximation, at the grand thermodynamic potential (density) $[\Omega = -\ln Z / (\beta V)]$

$$\Omega = \frac{1}{2} g_{BB} n_B^2 - \mu_B n_B + \Omega_F \left\{ = -\frac{\Delta^2}{U} + \frac{1}{V} \sum_{\mathbf{k}} [\xi_{\mathbf{k}} - E_{\mathbf{k}} + 2\beta^{-1} \ln f(-E_{\mathbf{k}})] \right\} \quad (3)$$

for a mixture with Bose particle number density n_B and Fermi particle number density

$$n_F = \frac{1}{V} \sum_{\mathbf{k}} \left[1 - \frac{\xi_{\mathbf{k}}}{E_{\mathbf{k}}} \tanh \frac{\beta E_{\mathbf{k}}}{2} \right], \quad (4)$$

where $E_{\mathbf{k}} = \sqrt{\xi_{\mathbf{k}}^2 + \Delta^2}$ is the quasiparticle energy, and $f(\varepsilon) = 1/(e^{\varepsilon/k_B T} + 1)$ is the standard Fermi-Dirac distribution. Alternatively, we can write Ω_F defined in Eq. (3) as a Landau-Ginzburg expansion in terms of the order parameter Δ according to

$$\Omega_F = \alpha_0 + \alpha_2 \Delta^2 + \frac{\alpha_4}{2} \Delta^4 \dots \quad (5)$$

where

$$\alpha_0 = \frac{2}{V\beta} \sum_{\mathbf{k}} \ln f(-\xi_{\mathbf{k}}), \quad (6a)$$

$$\alpha_2 = -\frac{1}{U} - \frac{1}{2V} \sum_{\mathbf{k}} \frac{1 - 2f(\xi_{\mathbf{k}})}{\xi_{\mathbf{k}}}, \quad (6b)$$

$$\alpha_4 = \frac{1}{V} \sum_{\mathbf{k}} \frac{1}{4\xi_{\mathbf{k}}^2} \times \left\{ \frac{1 - 2f(\xi_{\mathbf{k}})}{\xi_{\mathbf{k}}} - 2\beta f(\xi_{\mathbf{k}}) [1 - f(\xi_{\mathbf{k}})] \right\}. \quad (6c)$$

Equations (3) and (5) serve as the foundations for our studies below.

III. PHASE DIAGRAMS IN CHEMICAL POTENTIAL SPACE

In this section, we aim to gain a systematic understanding of the phase diagrams at finite temperature. An immediate obstacle to our goal is the existence of a large number of free parameters in our model. In order to alleviate this difficulty, we introduce a parameter $A = \hbar^2 (3\pi^2)^{2/3} / 2m_F$ which has the physical meaning that $An_F^{2/3}$ equals the Fermi energy ϵ_F , and adopt a unit system generalized from Ref. [12], in which several key parameters are scaled according to

$$\bar{\Omega} = \frac{g_{BF}^{10} \Omega}{g_{BB}^5 A^6}, \bar{\mu}_B = \frac{g_{BF}^5 \mu_B}{g_{BB}^3 A^3}, \bar{\mu}_F = \frac{g_{BF}^4 \mu_F}{g_{BB}^2 A^3},$$

$$\bar{n}_B = \frac{g_{BF}^5 n_B}{g_{BB}^2 A^3}, \bar{n}_F = \frac{g_{BF}^6 n_F}{g_{BB}^3 A^3}, \bar{k} = \frac{g_{BF}^2 k}{g_{BB} A}.$$

Additionally, Δ , μ , $k_B T$, and $\epsilon_{\mathbf{k}}$ are scaled same as μ_F , and the interaction between fermions of opposite spins [$\bar{U}_0 = U_0/(g_{BF}^2/g_{BB})$] is measured relative to g_{BF}^2/g_{BB} - the magnitude of induced fermion-fermion interaction due to the density fluctuation of Bose condensate [12]. As can be seen, the three original free parameters (g_{BF}, g_{BB}, U_0) are now reduced into a single scaled parameter \bar{U}_0 , making this unit system particularly suitable for studies aimed at identifying features generic to all the phase diagrams. To gain a qualitative understanding of this unit system, we note that for a mixture of ^{87}Rb and ^{84}Rb with $a_{BB} = 100a_0$ and $a_{BF} = 550a_0$ where a_0 is the Bohr radius [21], the unit is $1.61 \times 10^{-49} \text{ J m}^3$ for U_0 , ($2.15 \times 10^{-30} \text{ J}$, $3.84 \times 10^{-31} \text{ J}$) for (μ_F, μ_B) , ($1.34 \times 10^{19} \text{ m}^{-3}$, $7.49 \times 10^{19} \text{ m}^{-3}$) for

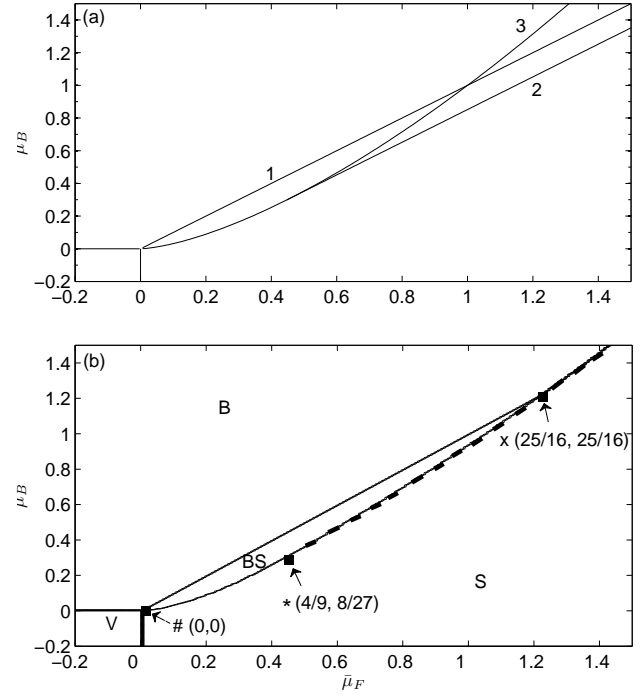


FIG. 1: (a) is the illustration designed to aid the understanding of the zero-temperature phase diagram in (b) where $U_0 = -1.126$. Units are defined in the text.

(n_F, n_B), and 156 nK for T . (However, for notational simplicity, same symbols will be used to stand for the scaled variables throughout the rest of the paper.)

Figures 1(b) and 2 showcase the features that are characteristic of both the zero- and the finite-temperature phase diagrams for a typical system within the validity of our model. They are constructed numerically by minimizing the potential in Eq. (3) with respect to n_B and Δ , which amounts to analyzing the saddle point equations and the relevant Hessian matrix [16, 17], as well as comparing, in the coexistence regions, the thermodynamic potentials of the possible phases listed below:

(V) for an empty phase where both $n_B = 0$ and $n_F = 0$,

(B) for a pure boson phase where $n_B \neq 0$ and $n_F = 0$,

(N) for a normal state of Fermi gas where $n_B = 0$, $\Delta = 0$, and $n_F \neq 0$,

(S) for a superfluid Fermi gas where $n_B = 0$, $\Delta \neq 0$, and $n_F \neq 0$,

(BN) for a normal Fermi-Bose mixture where $n_B \neq 0$, $\Delta = 0$, and $n_F \neq 0$, and finally

(BS) for a superfluid Fermi-Bose mixture where $n_B \neq 0$, $\Delta \neq 0$, and $n_F \neq 0$.

In order to capture the physics, making the study of phase diagrams more illuminating, we complement our numerical study with an analysis founded on the Landau-Ginzburg theory in the low temperature limit $T \ll \mu$. In this limit, α_4 [Eq. (8c) below] is always positive, and

we only need to consider the Landau-Ginzburg expansion up to the fourth order in Δ ,

$$\Omega = \frac{1}{2}n_B^2 - \mu_B n_B + \alpha_0(\mu, T) + \alpha_2(\mu, T)\Delta^2 + \frac{\alpha_4(\mu, T)}{2}\Delta^4, \quad (7)$$

where the integrals for the Landau coefficients in Eqs. (6) can be evaluated explicitly with the results [22]

$$\alpha_0 = -\mu^{5/2} \left[\frac{2}{5} + \frac{\pi^2}{4} \left(\frac{T}{\mu} \right)^2 \right], \quad (8a)$$

$$\alpha_2 = -\frac{1}{U_0} + \frac{3}{4}\mu^{1/2} \ln \frac{\pi T}{8\mu e^{\gamma-2}}, \quad (8b)$$

$$\alpha_4 = \frac{21}{32}\mu^{1/2} \frac{\zeta(3)}{T^2}, \quad (8c)$$

with $\gamma \approx 0.577$ being the Euler's constant. Further, in the same limit, we can ignore the thermal population in comparison with the population inside the Fermi sphere so that the Fermi density can be approximated as

$$n_F = -\frac{\partial \Omega}{\partial \mu_F} = \mu^{3/2} \left[1 + \frac{\pi^2}{8} \left(\frac{T}{\mu} \right)^2 \right] \simeq \mu^{3/2}, \quad (9)$$

Equations (8) and (9) form the backbone of the analytical discussions that we carry out below.

Consider first the mixed phase where both n_B and n_F have finite values. We begin with the saddle-point equation for n_B

$$n_B - \mu_B + \mu^{3/2} = 0, \quad (10)$$

which, when the use of $\mu = \mu_F - n_B$ is made, leads to a cubic equation for $\sqrt{\mu}$

$$(\sqrt{\mu})^3 - (\sqrt{\mu})^2 + (\mu_F - \mu_B) = 0. \quad (11)$$

The positive root to Eq. (11) that lies below $2/3$ (or $\sqrt{\mu} < 2/3$) represents a local stable mixed phase, where the inequality is derived by subjecting Eq. (7) to the local stability criteria that $\partial^2 \Omega / \partial n_B^2$ be positive. A simple analysis then shows that Eq. (11) supports the local stable mixed phase in the chemical potential space between the line [labeled as 1 in Fig. 1(a)]:

$$\mu_B = \mu_F, \quad (12)$$

and the parallel line [labeled as 2 in Fig. 1(a)] shifted with respect to Eq. (12) by $4/27$:

$$\mu_B = \mu_F - 4/27. \quad (13)$$

Next, consider the pure Bose phase described by the bosonic potential $\Omega_B = n_B^2/2 - \mu_B n_B$ and the pure Fermi phase described by the fermionic potential $\Omega_F = -\frac{2}{5}\mu_F^{5/2}$. In the region that supports the pure Fermi (Bose) phase, the effective chemical potential for fermions $\mu_F - n_B$

(bosons $\mu_B - n_F$) must be negative. As a result, the pure Bose phase exists above the line in Eq. (12), and the pure Fermi phase exists below the curve [labeled as 3 in Fig. 1(a)]

$$\mu_B = \mu_F^{3/2}. \quad (14)$$

It is then clear that the pure Fermi phase coexists with the mixed phase in the region below curve 3 but between lines 1 and 2, and it also overlaps with the pure Bose phase in the upper right region below curve 3 and above line 1.

So far, nothing has been said regarding the nature of the Fermi gas component. To answer this question, we go to the saddle point equation for Δ^2

$$\Delta^2 = -\frac{\alpha_2(\mu, T)}{\alpha_4(\mu, T)}. \quad (15)$$

Evidently, because $\alpha_4(\mu, T)$ is always positive, only when $\alpha_2(\mu, T) < 0$ does BCS order or superfluidity occur. Let $\mu_F^\#$ be the root to the threshold condition

$$\alpha_2(\mu_F^\#, T) = -\frac{1}{U_0} + \frac{3}{4}\sqrt{\mu_F^\#} \left(\ln \frac{\pi T}{8\mu_F^\# e^{\gamma-2}} \right) = 0. \quad (16)$$

In the limit where T goes to zero, $\mu_F^\#$ also goes to zero, and hence as expected under the attractive Fermi-Fermi interaction, fermions at $T = 0$ either exist as a pure S state or mix with bosons to form a mixed BS state.

Finally, by comparing the energies of the phases in each coexistent region, we change Fig. 1(a) into the phase diagram in Fig. 1(b), which features a tricritical point (labeled as $*$) at which the transition between BS and S changes from the second- to first-order type, and a critical point (labeled as \times) at which the second-order transition line between B and BS and the two first-order transition lines between S and, respectively, BS and B meet. The explanations are provided as follows. The first-order transition line (dotted) between B and S is given by

$$\mu_B = \sqrt{4/5}\mu_F^{5/4}, \quad (17)$$

which is obtained by setting $\Omega_B = \Omega_F$. The interception between Eq. (12) and Eq. (17) defines the critical point ($\mu_F^\times = \mu_B^\times = 25/16$). The comparison between Ω and Ω_F determines the first-order transition between BS and S, which starts from the critical point \times and ends at the tricritical point $*$ with ($\mu_F^* = 4/9, \mu_B^* = 8/27$) at which $n_B = \partial \Omega / \partial n_B = \partial^2 \Omega / \partial n_B^2 = 0$.

Note that for a single-component model with the repulsive Bose-Fermi interaction, the phase diagram at $T = 0$ has the same structure as Fig.1(b) except that S and BS are replaced, respectively, with N and BN, owing to the absence of pairing mechanism for fermions [11]. As stressed in the introduction, an advantage of the phase diagram in the chemical potential space is that each phase

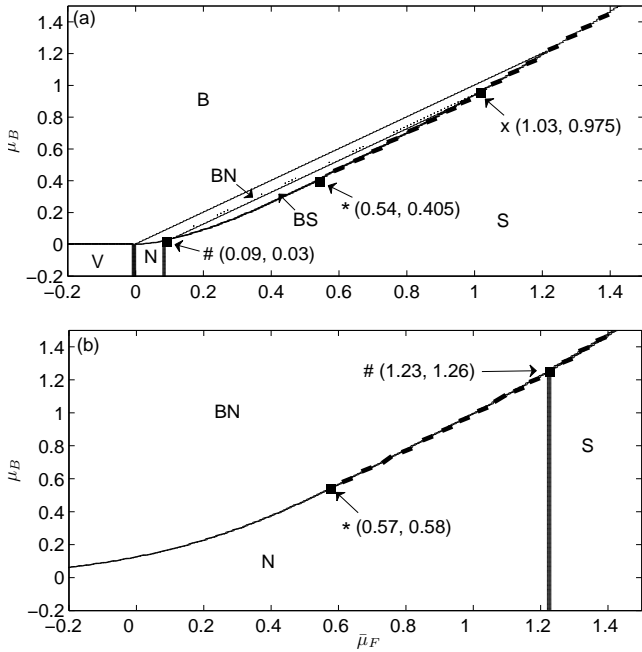


FIG. 2: The phase diagram (a) at $T = 0.001$ and (b) at $T = 0.25$. U_0 is same as in Fig. 1, and units are defined in the text.

separation manifests itself as a unique coexistence curve, making its identification particularly transparent. For example, Fig. 1 (b) automatically rules out phase separations other than those between a pure Fermi and a pure Bose phase and between a pure Fermi and a mixed phase. Thus, there is no need to hypothesize and analyze the existence of, for example, a phase separation between a pure bosonic and a mixed phase or that between two different mixed phases, as did in works where phase analysis was performed in space made up of particle number densities [15, 18].

At (low) finite temperature [Fig. 2(a)], the pure Fermi phase is divided into N and S by the vertical (second-order transition) line $\mu_F = \mu_F^\#$, where $\mu_F^\#$ increases with temperature according to Eq. (16), and the mixed phase is split into BN and BS by the (second-order transition) line, $\mu_B = \mu_F + n_F^\# - \mu_F^\#$, which begins at point # and ends at point x, with $n_F^\#$ being the Fermi number density [Eq. (4)] at $\Delta = 0$ and $\mu = \mu_F^\#$. As the temperature increases, both the N and BN region expand while S and BS contracts. A further increase in the temperature so that $\mu_F^\#$ lies beyond μ_F^* at the tricritical point results in a complete elimination of the phase space for the superfluid Fermi-Bose (BS) mixture as shown in Fig. 2(b), where the normal state Fermi-Bose mixture remains as the only mixed phase.

At this point, we recall that our analysis rests upon an assumption that the term $\pi^2 T^2 / 8\mu^2$ in Eq. (9) be much

less than 1, which is therefore applicable only to situations where the Fermi surface is well defined (relative to the temperature of interest). At zero temperature, the Fermi surface is fixed by $\mu = 4/9$ for line 2 (and the tricritical point), but is not defined for line 1 where $\mu = 0$; line 1 holds only for $T = 0$. As a result, the line dividing BN and BS in Fig. 2(a) (which corresponds to line 1 at zero temperature in Fig. 1) is far more sensitive to the temperature increase than the first-order transition line (and the tricritical point).

The line between B and BN requires a special explanation. At zero temperature, due to the Fermi-Dirac distribution, the chemical potential for a normal state of Fermi gas must be positive, and under such a circumstance, the pure Bose phase (B) is well-defined - the space above line 1, where the chemical potential is negative $\mu < 0$, is defined as the phase B. As temperature increases, the Fermi surface becomes less sharply defined, and so does the distinction between B and BN. In fact, at finite temperature there is nothing to prevent the chemical potential for fermions from becoming negative, just as for distinguishable particles that follow the Maxwell's distribution. In our study here, the line between B and BN is defined in such a way that the Fermi density along this line is 10^{-12} , a small threshold artificially introduced to indicate that the region in B is virtually free of fermions. But, we stress that in contrast to the line between BN and BS across which there is a second-order phase transition due to the emergence of the order parameter Δ which breaks the symmetry, there is no real phase transition for fermions across the line between B and BN.

IV. AN APPLICATION: TIGHTLY TRAPPED FERMIONS EMBEDDED IN A LARGE BEC

In practice, phase diagrams come in different forms, depending on the application at hands. A complete mapping of the phase diagram including all the critical points in the chemical potential space as we have done in the previous section is significant, not only because it provides a roadmap for constructing phase diagrams in other spaces, but also because it can greatly facilitate both the identification and the interpretation of the important features emerging from these diagrams. As an application, we consider, in this section, a double species experiment in which spherically symmetric harmonic trap potentials, $V_{B,F}(r)$, are tuned to differ in such a manner that fermions are tightly confined inside a much larger BEC, and use it as a model to explore how the surrounding bosons affect the physics of Fermi pairing. This model is the two-component analog of the single-component system experimentally realized by the MIT group in 2002 [4]. It also represents an example in which the traps are oppositely arranged compared to those adopted to implement the idea of using a small trapped BEC to probe the properties of a large Fermi gas component [17, 23].

In our study below, we assume that the Fermi component, although small compared to the BEC, is still sufficiently large so that the local-density approximation is directly applicable. Thus, for fermions, we introduce a local chemical potential $\mu_F(r) = \mu_F - V_F(r)$, in addition to a global chemical potential μ_F , which is fixed by the total particle number. In contrast, for bosons, owing to its large size, to a good approximation, we can regard its chemical potential, within the distance scale in the order of the size of the Fermi gas, to be a constant, μ_B , independent of the variation of the radial distance r .

Figure 3 (a) displays the phase diagram for a homogeneous system in the $T - \mu_F$ space for $\mu_B = 0.35$ [slightly smaller than μ_B^* in Fig. 2(a)]. At a given temperature and within the local-density approximation, a potential profile $V_F(r)$ along the radially outward direction in the real space induces an image $\mu_F(r)$ in the form of a vertical line moving down an arrow as indicated in Fig. 3. Then, by traversing from the tail to the head of the arrow and translating each point $[\mu_F(r)]$ on the vertical line into the density via the mapping $\rho_F^h(\mu_F(r))$, we can construct, from the center to the edge of the trap, the density distribution $\rho_F(r) \equiv \rho_F^h(\mu_F(r))$, where $\rho_F^h(x)$ calculates the Fermi density for a homogeneous phase at the chemical potential x . Using the rules just outlined and given the locations and the sizes of the vertical lines indicated in Fig. 3(a), we can easily arrive at the following qualitative conclusions.

(a) At sufficiently high temperature (the arrow on the right), the density profile consists of a normal phase (N) core surrounded by a (spherical) shell of a BN mixture.

(b) As temperature is lowered (the arrow in the middle), superfluidity (S) emerges from the core with N being sandwiched between S and BN.

(c) As temperature is further reduced (the arrow on the left), N disappears and substituted in its place is the Bose-superfluidity mixture (BS).

(d) A further reduction in the temperature completely eliminates BN , creating a density profile, reminiscent of the high temperature case in (a), except that N and BN in (a) are now replaced with S and BS , respectively.

An intriguing aspect of such a mixture is that both critical temperatures and Fermi profiles depend strongly on μ_B - the chemical potential of the surrounding BEC. As μ_B can be independently tuned in experiments, we have at our disposal a convenient tool to selectively access the parts of phase diagrams, that are physically interesting. Suppose that we want to access the first-order phase transition. We can do so simply by increasing μ_B beyond a certain threshold value. An example is given in Fig. 3(b) where μ_B is fixed to 0.45, a value slightly higher than μ_B^* in Fig. 2(a). As can be seen, part of the transition line dividing pure and mixed states changes its nature from second order in Fig. 3(a) to first order in Fig. 3(b). Thus, although the system can undergo a similar set of phase transitions as in Fig. 3(a) [at the expense of a higher Fermi chemical potential (or density) and a

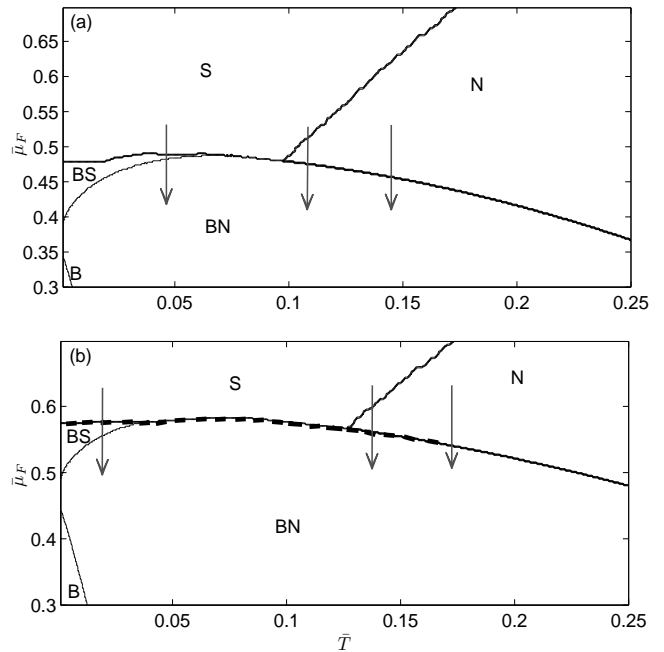


FIG. 3: The phase diagram in the $T - \mu_F$ space when the chemical potential for the bosons is fixed to (a) $\mu_B = 0.35$ and (b) $\mu_B = 0.45$. The features in (a) and (b) can be easily deduced from the phase diagrams in the previous section. U_0 is same as in Fig. 1, and units are defined in the text.

smaller BS region], a density discontinuity is expected to emerge from Fermi profiles on a sphere that divides the two phases sharing the same first-order transition line.

V. CONCLUSION

A unique advantage of a cold atom system is that its system parameters can be precisely tuned, allowing it to access a larger regime of phase diagrams. Further, availability of detection techniques, such as absorption laser imaging of densities and radio-frequency (RF) spectroscopy [24], makes the experimental determination of such phase diagrams in fine detail possible. In this work, we have performed a systematic study of the finite-temperature phase diagram in the chemical potential space for a two-component Fermi-Bose mixture with attractive Fermi-Fermi and repulsive Fermi-Bose interaction. Using a combination of scaling and Landau-Ginzburg theory, we have identified, within the framework of mean-field theory, a set of features generic to the phase diagrams for such mixtures. Further, we have applied the theory to explore the physics of pairing among fermions in a tightly confined trap surrounded by a large BEC gas.

Finally, we comment that so far, our analysis is based on the thermodynamic potential in Eq. (3) derived when all the phonon fields, $\phi_{\mathbf{k},B}(\tau)$, are ig-

nored. In more realistic situations, we need to retain the phonon fields, $\phi_{\mathbf{k},B}(\tau)$, which, after being explicitly integrated out under the Bogoliubov approximation, is shown to induce an attractive interaction, $U^{ind}(\mathbf{q}) = -g_{BF}^2/g_{BB}/\left[1 + (\hbar\mathbf{q}/\sqrt{4m_B g_{BB} n_B})^2\right]$, between fermions when the retardation effect is ignored [16, 25]. The net effect of $\phi_{\mathbf{k},B}(\tau)$ is then to change U_0 to $U^{eff} \equiv U_0 - g_{BF}^2/g_{BB}$, for the s-wave scattering, which is expected to dominate all the other partial-wave scatterings. Thus, the phase-diagram features presented in this work shall remain qualitatively true not only for two-component Fermi-Bose mixtures with direct Fermi-Fermi attraction ($U_0 < 0$), but also for those with di-

rect Fermi-Fermi repulsion ($U_0 > 0$) but attractive effective Fermi-Fermi interaction ($U^{eff} < 0$) [26]; the latter case turns out to cover several important systems of current experimental interest, including ^{40}K - ^{87}Rb and ^6Li - ^7Li [27].

VI. ACKNOWLEDGEMENT

This work is supported by the US National Science Foundation and US Army Research Office.

-
- [1] See, for instance, J. Bardeen, G. Baym, and D. Pines, Phys. Rev. Lett. **17**, 372 (1966); Phys. Rev. **156**, 207 (1967).
- [2] A.G. Truscott, K.E. Strecker, W.I. McAlexander, G.B. Patridge, and R.G. Hulet, Science **291**, 2570 (2001).
- [3] F. Schreck, L. Khaykovich, K.L. Corwin, G. Ferrari, T. Bourdel, J. Cubizolles, and C. Salomon, Phys. Rev. Lett. **87**, 080403 (2001).
- [4] Z. Hadzibabic, C.A. Stan, K. Dieckmann, S. Gupta, M.W. Zwierlein, A. Gorlitz, and W. Ketterle, Phys. Rev. Lett. **88**, 160401 (2002).
- [5] G. Ferrari et al., Phys. Rev. Lett. **89**, 053202 (2002).
- [6] G. Roati, F. Riboli, G. Modugno, and M. Inguscio, Phys. Rev. Lett. **89**, 150403 (2002).
- [7] S. Inouye, J. Goldwin, M. L. Olsen, C. Ticknor, J. L. Bohn, and D. S. Jin, Phys. Rev. Lett. **93**, 183201 (2004).
- [8] F. Ferlaino, C. D'Errico, G. Roati, M. Zaccanti, M. Inguscio, G. Modugno, and A. Simoni, Phys. Rev. A **73**, 040702(R) (2006).
- [9] B. Deh, C. Marzok, C. Zimmermann, and P. W. Courteille, Phys. Rev. A **77**, 010701(R) (2008).
- [10] C. A. Stan, M. W. Zwierlein, C. H. Schunck, S. M. F. Raupach, and W. Ketterle, Phys. Rev. Lett. **93**, 143001 (2004).
- [11] Y. - I. Shin, A. Schirotzek, C. H. Schunck, W. Ketterle, Phys. Rev. Lett. **101**, 070404 (2008)
- [12] L. Viverit, C. J. Pethick, and H. Smith, Phys. Rev. A **61**, 053605 (2000).
- [13] K. Mølmer, Phys. Rev. Lett. **80**, 1804 (1998).
- [14] G. V. Skorniakov and K. A. Ter-Martirosian, Zh. Eksp. Theor. Fiz. **31**, 775 (1956) [Sov. Phys. JETP **4**, 648 (1957)].
- [15] H. Heiselberg, C. J. Pethick, H. Smith, and L. Viverit, Phys. Rev. Lett. **85**, 2418 (2000).
- [16] M. J. Bijlsma, B. A. Heringa, and H. T. C. Stoof, Phys. Rev. A **61**, 053601 (2000).
- [17] B. Ramachandhran, S. G. Bhongale, and H. Pu, arXiv:0911.2487.
- [18] L. Salasnich and F. Toigo, Phys. Rev. A **75**, 013623 (2007).
- [19] L. Radzihovsky, P. B. Weichman, and J. I. Park, Ann. Phys. **323**, 2376 (2008).
- [20] John W. Negele and Henri Orland, Quantum Many-Particle Systems (Westview, Reading, MA, 1998).
- [21] J. P. Burke, Jr. and J. L. Bohn, Phys. Rev. A **59**, 1303 (1999).
- [22] E. M. Lifshitz and L. P. Pitaevskii, Statistical Physics, Part 2 (Pergamon, Oxford, 1980).
- [23] S. G. Bhongale and H. Pu, Phys. Rev. A **78**, 061606 (2008).
- [24] C. Chin, M. Bartenstein, A. Altmeyer, S. Riedl, S. Jochim, J. Hecker Denschlag, and R. Grimm, Science **305**, 1128 (2004).
- [25] Daw-Wei Wang, Phys. Rev. Lett. **96**, 140404 (2006).
- [26] L. Viverit, Phys. Rev. A **66**, 023605 (2002).
- [27] F. Illuminati and A. Albus, Phys. Rev. Lett. **93** 090406 (2004).